Inorg. Chem. **2003**, *42*, 641–649

Synthesis and Characterization of Heterodinuclear Ln^{3+}–Fe^{3+} and Ln^{3+}–Co^{3+} Complexes, Bridged by Cyanide Ligand (Ln^{3+} = Lanthanide Ions). Nature of the Magnetic Interaction in the Ln^{3+}–Fe^{3+} Complexes

Albert Figuerola,[†] Carmen Diaz,*[,†] Joan Ribas,[†] Vassilis Tangoulis,[‡] Jaume Granell,[†] Francesc Lloret,[§] José Mahía,[||] and Miguel Maestro[||]

Departament de Química Inorgànica, Universitat de Barcelona, Martí i Franqués 1-11,08028 Barcelona, Spain, Department of Materials Science, University of Patras, 26500 Patras, Greece, Departament de Química Inorgànica, Universitat de València, Doctor Moliner 50, 46100 Burjasot, Spain, and Servicios Xerais de Apoio á Investigación (SXAIN), Universidade da Coruña, Edificio anexo Facultade de Ciencias,15071 A Coruña, Spain

Received April 24, 2002

The reaction of $Ln(NO_3)_3$·aq with $K_3[Fe(CN)_6]$ or $K_3[Co(CN)_6]$ in *N*,*N*′-dimethylformamide (DMF) led to 25 heterodinuclear $[Ln(DMF)_4(H_2O)_3(\mu\text{-}CN)Fe(CN)_5]\cdot nH_2O$ and $[Ln(DMF)_4(H_2O)_3(\mu\text{-}CN)Co(CN)_5]\cdot nH_2O$ complexes (with Ln = all the lanthanide(III) ions, except promethium and lutetium). Five complexes (Pr^{3+}–Fe^{3+}), (Tm^{3+}–Fe^{3+}), (Ce^{3+}–Co^{3+}), (Sm^{3+}–Co^{3+}), and (Yb^{3+}–Co^{3+}) have been structurally characterized; they crystallize in the equivalent monoclinic space groups $P2_1/c$ or $P2_1/n$. Structural studies of these two families show that they are isomorphous. This relationship in conjunction with the diamagnetism of the Co^{3+} allows an approximation to the nature of coupling between the iron(III) and the lanthanide(III) ions in the $[Ln(DMF)_4(H_2O)_3(\mu\text{-}CN)Fe(CN)_5]\cdot nH_2O$ complexes. The Ln^{3+}–Fe^{3+} interaction is antiferromagnetic for Ln = Ce, Nd, Gd, and Dy and ferromagnetic for Ln = Tb, Ho, and Tm. For Ln = Pr, Eu, Er, Sm, and Yb, there is no sign of any significant interaction. The isotropic nature of Gd^{3+} helps to evaluate the value of the exchange interaction.

Introduction

The association of 3d−4f ions in cyanide-bridged low dimensional arrays is original and may open new perspectives for the use of the optical properties of rare earth ions included in magnetic molecular media.[1−3] In general, little is known about the nature of the exchange interactions of rare earth ions either with one another or with other magnetic groups. The major difficulties in analyzing the magnetic properties of the 3d−4f couples arise from the fact that the ground state of the Ln^{3+} ion, with the exception of Gd^{3+}, has a first-order angular momentum, which prevents the use of a spin-only Hamiltonian for isotropic exchange. The joint effects of the crystal field and orbital contribution can result in an important anisotropy of the magnetic susceptibility and exchange interactions. The crystal field splitting is usually of the order of *kT* at room temperature, so that the thermal dependence of the populations of the Stark levels has to be implicitly taken into account. To date, the studies addressing these problems in the case of 3d−4f molecular complexes are very scarce.[4−8]

Until recently, few compounds containing magnetically coupled 3d−4f molecular complexes were available. Most of them are Gd^{3+}−Cu^{2+} [8−13] or Gd^{3+}−radical organic

* To whom correspondence should be addressed. E-mail: carme.diaz@qi.ub.es.
[†] Universitat de Barcelona.
[‡] University of Patras.
[§] Universitat de Valencia.
[||] Universidade da Coruña.

(1) de Sá, G. F.; Malta, O. P.; de Mello Donegá, C.; Simas, A.; Longo, R. L.; Santacruz, P. A.; da Silva, E. F., Jr. *Coord. Chem. Rev.* **2000**, *196*, 165 and references therein.
(2) Kahn, M. L.; Mathonière, C.; Kahn, O. *Inorg. Chem.* **1999**, *38*, 3692.
(3) Costes, J. P.; Dahan, F.; Dupuis, A.; Laurent, J. P. *Inorg. Chem.* **2000**, *39*, 169.
(4) Benelli, C.; Caneschi, A.; Gatteschi, D.; Guillou, O.; Pardi, L. *Inorg. Chem.* **1990**, *29*, 1750.
(5) Sanz, J. L. Ruiz,L.; Gleizes, A.; Lloret, F.; Faus, J.; Julve, M.; Borras-Almenar, J. J.; Journaux, Y. *Inorg. Chem.* **1996**, *35*, 7384.
(6) Levy, P. M. *Phys. Rev.* **1966**, *147*, 147.
(7) Kamimura, H.; Yamaguchi, Y. *Phys. Rev.* **1970**, *1*, 2002.
(8) Costes, J. P.; Dahan, F., Dupuis, A.; Laurent, J. P. *Chem. Eur. J.* **1998**, *4*, 1616.
(9) Benin, A.; Benelli, C.; Canneschi, A.; Carlin, R. L.; Dei, A.; Gatteschi, D. *J. Am. Chem. Soc.* **1985**, *107*, 812.

10.1021/ic025669g CCC: $25.00
Published on Web 12/24/2002

systems.[14−16] Among those with polycyanometalates and 4f ions, several compounds with different dimensionality have been reported: (a) three-dimensional polycyanometalates-(III) (Fe, Co, Cr);[17,18] (b) two-dimensional polycyanometalates(III) (Cr, Fe);[19,20] (c) one-dimensional polycyanometalates-(II) (Ni, Pt);[21,22] and (d) one-dimensional polycyanometalates-(III) (Fe, Co, Mn).[23−25] Recently, two one-dimensional derivatives from $[Cr(CN)_6]^{3-}$ and Gd^{3+}, *cis*-$[Cr(CN)_4(\mu\text{-}CN)_2Gd(H_2O)_2(DMF)_4]_n\cdot n H_2O$ and *trans*-$[Cr(CN)_4(\mu\text{-}CN)_2Gd(H_2O)_4(bpy)]_n\cdot 4nH_2O\cdot 1.5n$bpy, were published by the authors.[26] Discrete 3d−4f molecular complexes have also been published: (e) a trinuclear complex of formula $\{[Gd(DMA)_3(H_2O)_4]_2Fe(CN)_6\}\cdot 3H_2O$;[27] (f) dinuclear complexes of formula $[Ln(DMF)_4(H_2O)_2Mn(CN)_6]\cdot H_2O$ (Ln = Tb, Dy, Er),[28] (g) dinuclear complexes of formula $[Ln(DMF)_4(H_2O)_nFe(CN)_6]\cdot H_2O$ (Ln = La, Ce, Sm; $n = 4$)[29,30] (Ln = Er, Yb, Lu; $n = 3$).[31] Following this study of complexes with 3d−4f ions, we tried to start with discrete complexes, because the study of the exchange interactions, where the spin−orbit coupling is important, may be easier in these systems than in more extended ones.

The present work focuses on the study of the magnetic susceptibility of 25 complexes belonging to the homologous families $[Ln(DMF)_4(H_2O)_3(\mu\text{-}CN)Fe(CN)_5]\cdot nH_2O$ and $[Ln(DMF)_4(H_2O)_3(\mu\text{-}CN)Co(CN)_5]\cdot n\ H_2O$ (Ln represents all the lanthanides(III) ions except lutetium, which is diamagnetic, and promethium, which is radioactive; DMF = *N*,*N*′-dimethylformamide; $1 \leq n \leq 2$). All these compounds are isomorphous, and this relationship in conjunction with the diamagnetism of the Co^{3+} ion allows an approach to the nature of the coupling between the iron(III) and the lanthanide(III) ions. Structural characterization of $[Pr(DMF)_4(H_2O)_3(\mu\text{-}CN)Fe(CN)_5]\cdot H_2O$ (**1**), $[Tm(DMF)_4(H_2O)_3(\mu\text{-}CN)Fe(CN)_5]\cdot 1.25H_2O$ (**2**), $[Yb(DMF)_4(H_2O)_3(\mu\text{-}CN)Co(CN)_5]\cdot 1.5H_2O$ (**3**), $[Ce(DMF)_4(H_2O)_3(\mu\text{-}CN)Co(CN)_5]\cdot H_2O$ (**4**), and $[Sm(DMF)_4(H_2O)_3(\mu\text{-}CN)Co(CN)_5]\cdot 2H_2O$ (**5**) complexes is reported.

Experimental Section

Materials. All starting materials were purchased from Aldrich and were used without further purification.

Syntheses. For the investigation reported here, we prepared two series of dinuclear $Ln^{3+}-Fe^{3+}$and $Ln^{3+}-Co^{3+}$ complexes, where Ln represents any ion of the 4f family, except promethium which is radioactive and lutetium which is diamagnetic.

$[Ln(DMF)_4(H_2O)_3(\mu\text{-}CN)Fe(CN)_5]\cdot nH_2O$ ($1 \geq n \geq 1.5$). The $Ln^{3+}-Fe^{3+}$ complexes were obtained by adding a solution of $Ln(NO_3)_3\cdot nH_2O$ ($n = 5$, 6) (0.78 mmol) in *N*,*N*′-dimethylformamide (DMF) (25 mL) to an equimolar solution of $K_3[Fe(CN)_6]$ in water (25 mL). The solutions were left undisturbed, and well-formed orange crystals were obtained, for all of them, after several days (yield ca. 70%).

$[Ln(DMF)_4(H_2O)_3(\mu\text{-}CN)Co(CN)_5]\cdot nH_2O$ ($1 \geq n \geq 2$). The $Ln^{3+}-Co^{3+}$ complexes were obtained by the same procedure using $K_3[Co(CN)_6]$ instead of $K_3[Fe(CN)_6]$. Well-formed colorless or light-colored crystals (depending on the lanthanide ion) were obtained, for all of them, after several days (yield ca. 70%).

Elemental analyses (C, N, H) were consistent with the formulation. Their IR spectra show a group of narrow and strong bands between 2100 and 2200 cm^{-1}. These bands correspond to the stretching frequency ν(CN), and the fact that there is more than one band indicates that the CN^- ligand has more than a single coordination mode: one mode is a bridge, and one is a terminal ligand. There is another group of overlapped strong bands between 1600 and 1700 cm^{-1}, corresponding to the stretching frequency ν(CO) and confirming the presence of *N*,*N*′-dimethylformamide molecules.

Studies of their reactivity showed the following: (a) slow evaporation of aqueous solutions of these heterodinuclear complexes results in the isolation of three-dimensional (3D) complexes of formula $LnFe(CN)_6\cdot nH_2O$ and $LnCo(CN)_6\cdot nH_2O$, previously described by Huliger et al.[17−18] (b) Their reaction in aqueous solution with 2,2′-bipyridine results in the isolation of one-dimensional (1D) complexes of formula *trans*-$[M(CN)_4(\mu\text{-}CN)_2Ln(H_2O)_4(bpy)]_n\cdot 4nH_2O\cdot 1.5n$bpy (M = Co^{3+}, Fe^{3+}; Ln = lathanide(III) ions; bpy = *2,2*′-bipyridine) analogous to that already reported by us, with M = Cr^{3+} and Ln = Gd^{3+}.[26]

X-ray Structure Determination. Crystal data and details on the data collection and refinement are summarized in Table 1. Suitable crystals of $[Pr^{3+}-Fe^{3+}]$ (**1**) (irregular, yellow, dimensions 0.35 × 0.20 × 0.10 mm^3), $[Tm^{3+}-Fe^{3+}]$ (**2**) (block, yellow, dimensions 0.50 × 0.50 × 0.30 mm^3), $[Yb^{3+}-Co^{3+}]$ (**3**) (block, colorless, dimensions 0.50 × 0.45 × 0.35 mm^3), $[Ce^{3+}-Co^{3+}]$ (**4**) (block, colorless, dimensions 0.60 × 0.50 × 0.40 mm^3), and $[Sm^{3+}-Co^{3+}]$ (**5**) (block, colorless, dimensions 0.37 × 0.26 × 0.20 mm^3) were used for the structure determination. X-ray data were collected using a Bruker SMART CCD area detector single-crystal diffractometer with graphite monochromatized Mo Kα radiation (λ = 0.71073 Å) by the $\varphi-\omega$ scan method at 173(2) K. A total of 1271 frames

(10) Blake, A.; Milne, P. E.; Winpenny, R. E. P. *Angew. Chem., Int. Ed. Engl.* **1991**, *30*, 1139.
(11) Liang, Y.; Cao, R.; Su, W.; Hong, M.; Zhang, W. *Angew. Chem., Int. Ed.* **2000**, *39*, 3304.
(12) Ryazanov. M.; Nikiforov, V.; Lloret, F.; Julve, M.; Kuzmina, N.; Gleizes, A. *Inorg. Chem.* **2002**, *7*, 1816.
(13) Tang, J. K.; Li, Y. Z.; Wang, Q. L.; Gao, E. Q.; Liao, D. Z.; Jiang, Z. H.; Yan, S. P.; Cheng, P.; Wang, L. F.; Wang, G. L. *Inorg. Chem.* **2002**, *8*, 2188.
(14) Guillou, O.; Kahn, O.; Oushoorn, R. L.; Boubekeur, K.; Batail, P. *Angew. Chem., Int. Ed. Engl.* **1992**, *31*, 626.
(15) Sutter, J. P.; Kahn, M. L.; Golhen, S.; Ouahab, L.; Kahn, O. *Chem. Eur. J.* **1998**, *4*, 571.
(16) Canneschi, A.; Dei, A.; Gatteschi, D.; Sorace, L.; Vostrikova, K. *Angew. Chem., Int. Ed.* **2000**, *39*, 246.
(17) Huliger, F.; Landolt, M.; Vetsch, H. *J. Solid State Chem.* **1976**, *18*, 307.
(18) Huliger, F.; Landolt, M.; Vetsch, H. *J. Solid State Chem.* **1976**, *18*, 283.
(19) Kou, H. Z.; Gao, S.; Jin, X. *Inorg. Chem.* **2001**, *40*, 6295.
(20) Ma, B. Q.; Gao, S.; Su, G.; Xu, G. X. *Angew. Chem., Int. Ed.* **2001**, *40*, 434.
(21) Knoeppel, D. W.; Liu, J.; Meyers, E. A.; Shore, S. G. *Inorg. Chem.* **1998**, *37*, 4828.
(22) Du, B.; Ding, E.; Meyers, E. A.; Shore, S. G. *Inorg.Chem.* **2001**, *40*, 3637.
(23) Yan, B.; Wang, H. D.; Chen, Z. D. *Polyhedron* **2001**, *20*, 591.
(24) Yan, B.; Chen, Z.; Wang, S.; Gao, S. *Chem. Lett.* **2001**, 350.
(25) Tanase, S.; Andruh, M.; Müller, A.; Schmidtmann, M.; Mathonière, C.; Rombaut, G. *Chem. Commun.* **2001**, 1084.
(26) Figuerola, A.; Diaz, C.; Ribas, J.; El. Falah, M. S.; Maestro, M.; Mahía, J. *Chem. Commun.* **2001**, 1204.
(27) Yan, B.; Chen, Z. *Helv. Chim. Acta* **2001**, 817.
(28) Yan, B.; Chen, Z. *Transition Met. Chem. (Dordrecht, Neth.)* **2001**, *26*, 287.
(29) Kautz, J. A.; Mullica, D. F.; Cunningham, B. P.; Combs, R. A.; Farmer, J. M. *J. Mol. Struct.* **2000**, *523*, 175.
(30) Kou, H. Z.; Yang, G. M.; Liao, D. Z.; Cheng, P.; Jiang, Z. H.; Yan, S. P.; Huang, X. Y.; Wang, G. L. *J. Chem. Crystallogr.* **1998**, *28*, 303.
(31) Mullica, D. F.; Farmer, J. M.; Cunningham, B. P.; Kautz, J. A. *J. Coord. Chem.* **2000**, *49*, 239.

Table 1. Crystal Parameters for **1**−**5**

	[$Pr^{3+}-Fe^{3+}$] (**1**)	[$Tm^{3+}-Fe^{3+}$] (**2**)	[$Yb^{3+}-Co^{3+}$] (**3**)	[$Ce^{3+}-Co^{3+}$] (**4**)	[$Sm^{3+}-Co^{3+}$] (**5**)
empirical formula	$C_{18}H_{36}FeN_{10}O_8Pr$	$C_{18}H_{36.5}FeN_{10}O_{8.25}Tm$	$C_{18}H_{37}CoN_{10}O_{8.5}Yb$	$C_{18}H_{36}CeCoN_{10}O_8$	$C_{18}H_{38}CoN_{10}O_9Sm$
formula mass	717.33	749.85	761.55	719.62	747.86
space group	$P2_1/n$	$P2_1/c$	$P2_1/c$	$P2_1/n$	$P2_1/n$
cryst syst	monoclinic	monoclinic	monoclinic	monoclinic	monoclinic
Z	4	4	4	4	4
a, Å	17.532(1)	13.888(1)	13.836(1)	17.385(1)	17.437(1)
b, Å	8.881(1)	8.842(1)	8.812(1)	8.880(1)	8.841(1)
c, Å	19.834(1)	24.747(1)	24.588(1)	19.893(1)	19.812(2)
β, deg	95.795(1)	96.695(1)	96.811(1)	95.957(1)	96.031(1)
V, Å^3	3072.9(1)	3018.3(1)	2976.5(1)	3054.51(1)	3037.3(4)
ρ(calcd), g/cm^3	1.551	1.650	1.699	1.565	1.635
μ_{calcd}, mm^{-1}	2.093	3.457	3.738	2.068	2.519
radiation (Mo Kα), Å	0.71073	0.71073	0.71073	0.71073	0.71073
T, K	173(2)	173(2)	173(2)	173(2)	173(2)
θ range for data collection	1.5−28.3	1.5−28.3	1.5−28.3	1.5−28.3	1.48−28.30
final R indices[a]	R1 = 0.0313	R1 = 0.0262	R1 = 0.0388	R1 = 0.0322	R1 = 0.0317
[$I > 2\sigma(I)$]	wR2 = 0.0655	wR2 = 0.0575	wR2 = 0.0932	wR2 = 0.0820	wR2 = 0.0892
final R indices	R1 = 0.0477	R1 = 0.0293	R1 = 0.0432	R1 = 0.0368	R1 = 0.0441
[for all data]	wR2 = 0.0710	wR2 = 0.0585	wR2 = 0.0951	wR2 = 0.0846	wR2 =0.0976

[a] $R1 = \sum||F_o| - |F_c||/\sum|F_o|$ and $wR2 = \{\sum[w(F_o^2 - F_c^2)^2]/\sum[w(F_o^2)^2]\}^{1/2}$.

of intensity data were collected for each compound. The first 50 frames were recollected at the end of data collection to monitor for decay. In each case, the crystals used for the diffraction studies showed no decomposition during data collection. The integration process yielded a total of 16540 reflections for **1**, 19939 for **2**, 19416 for **3**, 20583 for **4**, and 20841 for **5**, of which 7514 [R(int) = 0.0435], 7432 [R(int) = 0.0201], 7317 [R(int) = 0.0414], 7533 [R(int) = 0.0372], and 7499 [R(int) = 0.0325], respectively, were independent. Absorption corrections were applied using the SADABS[32] program (maximum and minimum transmission coefficients, 1.000 and 0.436 for **1**; 1.000 and 0.701 for **2**; 1.000 and 0.503 for **3**; 1.000 and 0.494 for **4**; 0.6327 and 0.4558 for **5**). The structures were solved using the Bruker SHELXTL-PC[33] software by direct methods and refined by full-matrix least-squares methods on F^2. Hydrogen atoms were included in calculated positions and refined in the riding mode, except for those of water molecules that were located on residual density maps but then fixed their positions and refined in the riding mode. For **1**, convergence was reached at a final R1 = 0.0313 [for $I > 2\sigma(I)$], wR2 = 0.0710 [for all data], 359 parameters, with allowance for the thermal anisotropy for all non-hydrogen atoms. The weighting scheme employed was $w = [\sigma^2(F_o)^2 + (0.0183P)^2]$ and $P = (|F_o|^2+2|F_c|^2)/3$, and the goodness of fit on F^2 was 0.953 for all observed reflections. For **2**, convergence was reached at a final R1 = 0.0262 [for $I > 2\sigma(I)$], wR2 = 0.0585 [for all data], 352 parameters, with allowance for the thermal anisotropy for all non-hydrogen atoms. The weighting scheme employed was $w = [\sigma^2(F_o)^2 + (0.0159P)^2 + 5.1914P]$ and $P = (|F_o|^2+2|F_c|^2)/3$, and the goodness of fit on F^2 was 1.199 for all observed reflections. For **3**, convergence was reached at a final R1 = 0.0388 [for $I > 2\sigma(I)$], wR2 = 0.0951 [for all data], 360 parameters, with allowance for the thermal anisotropy for all non-hydrogen atoms. The weighting scheme employed was $w = [\sigma^2(F_o)^2 + (0.0332P)^2 + 9.1711P]$ and $P = (|F_o|^2+2|F_c|^2)/3$, and the goodness of fit on F^2 was 1.144 for all observed reflections. For **4**, convergence was reached at a final R1 = 0.0322 [for $I > 2\sigma(I)$], wR2 = 0.0846 [for all data], 351 parameters, with allowance for the thermal anisotropy for all non-hydrogen atoms. The weighting scheme employed was $w = [\sigma^2(F_o^2 + (0.0533P)^2 + 0.5369P]$ and $P = (|F_o|^2+2|F_o|^2)/3$, and the goodness of fit on F^2 was 1.001 for all observed reflections. For **5**, convergence was reached at a final R1 = 0.0317 [for $I > 2\sigma(I)$], wR2 = 0.0976 [for all data], 382 parameters, with allowance for the thermal anisotropy for all non-hydrogen atoms. The weighting scheme employed was $w = [\sigma^2(F_0^2) + (0.0533P)^2 + 5.3848P]$ and $P = (|F_0|^2+2|F_c|^2)/3$, and the goodness of fit on F^2 was 1.110 for all observed reflections. Crystallographic data (excluding structure factors) for the structures reported in this paper have been deposited with the Cambridge Crystallographic Data Centre as supplementary publications CCDC-175800 (**1**), CCDC-175801 (**2**), CCDC-175802 (**3**), CCDC-175803 (**4**), and CCDC-178105 (**5**). Copies of the data can be obtained free of charge on application to CCDC, 12 Union Road, Cambridge CB2 1EZ, U.K. (Fax: (+44)1223-336-033. E-mail: deposit@ccdc.cam.ac.uk.)

Physical Measurements. Magnetic data were collected on a powdered sample, for all the compounds, with a superconducting quantum interference device (SQUID) magnetometer.

Susceptibility measurements were made in a field of 1000 G, and magnetization measurements were made at 2 K. All data were corrected for diamagnetism estimated from Pascal's constants. Polycrystalline powder EPR spectra were recorded at X-band frequency (9.23 GHz) on a Varian ESR9 spectrometer equipped with a continuous flow ^{4}He cryostat.^{1}H NMR spectra at 250 MHz, in D_2O solution, were recorded on a Bruker DRX 250 spectrometer. The solid state ^{13}C cross polarization-MAS NMR spectra were recorded on a Varian 300 spectrometer, at a measurement frequency of 75.432 MHz and a rotation frequency of 4000 Hz. Chemical shifts (in ppm) were measured relative to hexamethylbenzene (external reference).

Results and Discussion

Description of the Structures of $[Pr(DMF)_4(H_2O)_3(\mu\text{-}CN)Fe(CN)_5]\cdot H_2O$ (1), $[Tm(DMF)_4(H_2O)_3(\mu\text{-}CN)Fe(CN)_5]\cdot 1.25H_2O$ (2), $[Yb(DMF)_4(H_2O)_3(\mu\text{-}CN)Co(CN)_5]\cdot 1.5H_2O$ (3), $[Ce(DMF)_4(H_2O)_3(\mu\text{-}CN)Co(CN)_5]\cdot H_2O$ (4), and $[Sm(DMF)_4(H_2O)_3(\mu\text{-}CN)Co(CN)_5]\cdot 2H_2O$ (5). The structure of these complexes was determined by X-ray crystallography. In all five cases, the crystal system is monoclinic with space group $P2_1/c$ or $P2_1/n$, and the unit cell contains four discrete heterodinuclear molecules (Table 1). A view of [$Ce^{3+}-Co^{3+}$]

(32) Sheldrick, G. M. *SADABS*; program for absorption corrections using Bruker CCD data; University of Göttingen: Göttingen, Germany, 1996.
(33) Sheldrick, G. M. *SHELXTL-PC*; Bruker; University of Göttingen: Göttingen, Germany, 1997.

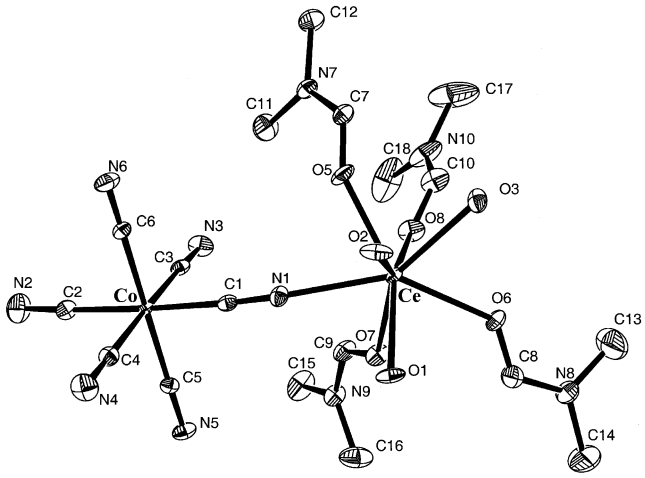

Figure 1. Molecular plot for [Ce^{3+}−Co^{3+}] (**4**) (ellipsoids drawn at 50% probability level).

Table 2. Selected Bonds Lengths (Å) and Angles (deg) for **1**−**5**

	1	**2**	**3**	**4**	**5**
Ln(1)−O(1)	2.466(2)	2.327(2)	2.325(3)	2.501(2)	2.440(3)
Ln(1)−O(2)	2.480(2)	2.337(2)	2.345(3)	2.500(2)	2.442(3)
Ln(1)−O(3)	2.480(2)	2.359(2)	2.316(3)	2.489(2)	2.426(3)
Ln(1)−O(5)	2.413(2)	2.350(2)	2.311(3)	2.444(2)	2.390(3)
Ln(1)−O(6)	2.454(2)	2.336(2)	2.312(3)	2.468(2)	2.416(3)
Ln(1)−O(7)	2.448(2)	2.318(2)	2.344(3)	2.435(2)	2.425(3)
Ln(1)−O(8)	2.428(2)	2.322(2)	2.324(3)	2.468(2)	2.385(3)
Ln(1)−N(1)	2.558(3)	2.394(2)	2.384(4)	2.579(2)	2.513(3)
M(1)−C(1)	1.937(3)	1.933(3)	1.886(4)	1.891(3)	1.899(4)
M(1)−C(2)	1.929(3)	1.938(3)	1.892(5)	1.889(3)	1.899(4)
M(1)−C(3)	1.932(3)	1.942(3)	1.899(4)	1.893(3)	1.900(4)
M(1)−C(4)	1.931(3)	1.951(3)	1.905(5)	1.896(3)	1.900(4)
M(1)−C(5)	1.939(3)	1.938(3)	1.895(4)	1.896(2)	1.893(4)
M(1)−C(6)	1.940(3)	1.938(3)	1.894(4)	1.894(2)	1.895(4)
C(1)−N(1)	1.149(4)	1.150(4)	1.146(6)	1.141(3)	1.152(5)
Ln(1)−N(1)−C(1)	164.2(3)	163.9(2)	164.2(4)	163.0(2)	163.5(5)
M(1)−C(1)−N(1)	176.8(3)	176.3(3)	176.1(4)	177.4(2)	177.9(6)

complex (**4**) is represented in Figure 1. Selected bond distances and angles are given in Table 2 for the five compounds. The structure consists of a cyano-bridged array of $M(CN)_6$ and $Ln(DMF)_4(H_2O)_3$ fragments forming heterobimetallic molecular entities linked by a CN^--bridged ligand. The Ln^{3+} atom is eight-coordinated with a distorted dodecahedral geometry. Seven oxygen atoms surround the Ln^{3+} ion: three of water and four of DMF molecules. The nitrogen atom of the bridging CN^- ligand occupies the eighth coordination position. The distances Ln−O range from 2.50 to 2.31 Å. The lowest values correspond to Tm and Yb in accordance with the variation of the atomic radium of the lanthanide ions. The longest Ln−ligand distance corresponds to the nitrogen atom of the CN^- bridge. Six cyanide ligands surround the M^{3+} (Co, Fe) ion in a distorted octahedral environment. The M−C distances range from 1.95 to 1.88 Å, and the lowest corresponds to the $[Co(CN)_6]^{3-}$. The intramolecular distances between the two metals through the CN^- bridge were Pr···Fe = 5.580 Å, Tm···Fe = 5.411 Å, Yb···Co = 5.352 Å, Ce···Co = 5.539 Å, and Sm···Co = 5.499 Å.

The neutral dinuclear units are linked by hydrogen bonds in a three-dimensional network. As an example, a projection of the packing for the [Pr^{3+}−Fe^{3+}] complex (**1**) in the *yz* and *xy* planes is shown in Figures 2 and 3, respectively. The

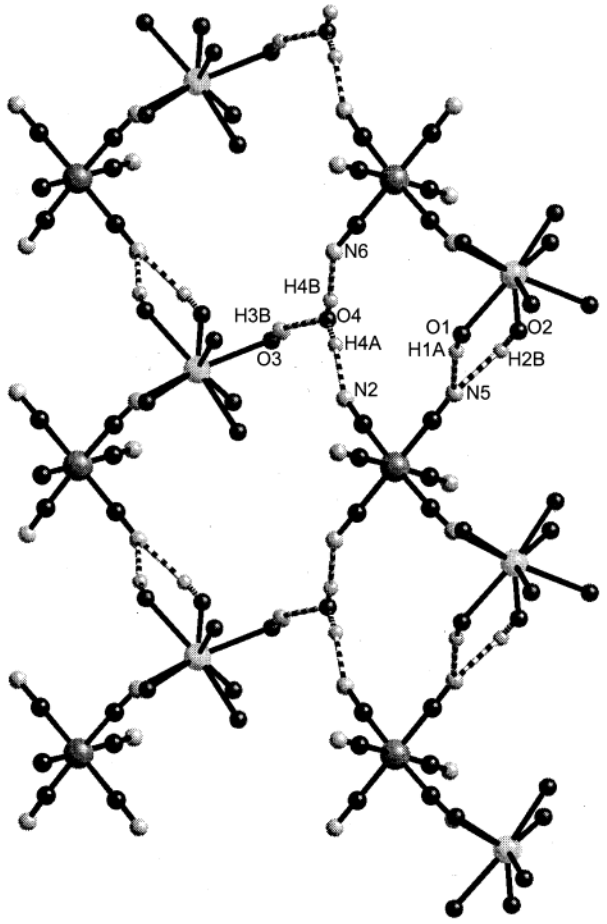

Figure 2. Projection of [Pr^{3+}−Fe^{3+}] (**1**) in the *yz* plane of the H-bonded 3D network.

3D network shows an alternation of [M−Ln] dinuclear entities linked by hydrogen bonds between the five terminal CN^- groups of the $M(CN)_6$ fragment, the three oxygen atoms of the H_2O ligand of the $Ln(DMF)_4(H_2O)_3$ fragment, and the water molecules of crystallization. Hydrogen bond distances and angles are shown for compounds **1**−**5** (Supporting Information, Table S1).

Isostructural Analysis. The X-ray powder diffractograms have been recorded for all compounds at room temperature in order to confirm their isostructurality along both series and also between them. Two structures determined by single-crystal X-ray diffraction have been used as structural models for each series: structures [Pr^{3+}−Fe^{3+}] (**1**) and [Tm^{3+}−Fe^{3+}]-(**2**) for the Ln^{3+}−Fe^{3+} family and structures [Yb^{3+}−Co^{3+}] (**3**) and [Ce^{3+}−Co^{3+}] (**4**) for the Ln^{3+}−Co^{3+} family. The diffractograms have been fitted by the Rietveld method[34] using the FULLPROF program.[35] After the conversion between the observed and the calculated diffractograms, we were able to confirm their isostructurality. The decrease in the cell parameters from La to Yb compounds is in complete agreement with the already well-established radii contraction of lanthanide ions from the beginning to the end of the rare

(34) Rietveld, M. H. *J. Appl. Crystallogr.* **1969**, *2*, 65.
(35) Rodriguez-Carvajal, J. *Abstracts of the Satellite Meeting on Power Diffraction of the XV Congres of the IUCr Toulouse, France*; 1990, 127.

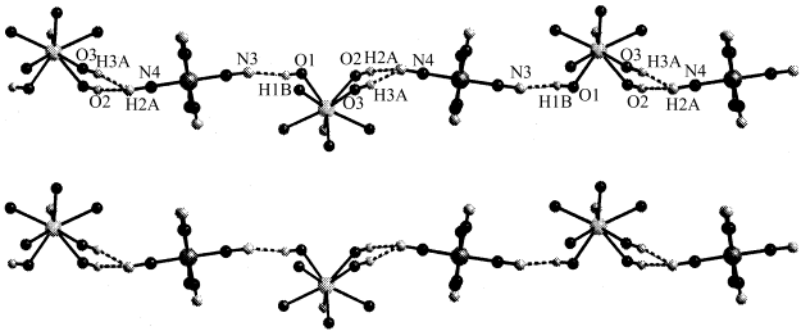

Figure 3. Projection of $[Pr^{3+}-Fe^{3+}]$ (**1**) in the *xy* plane of the H-bonded 3D network.

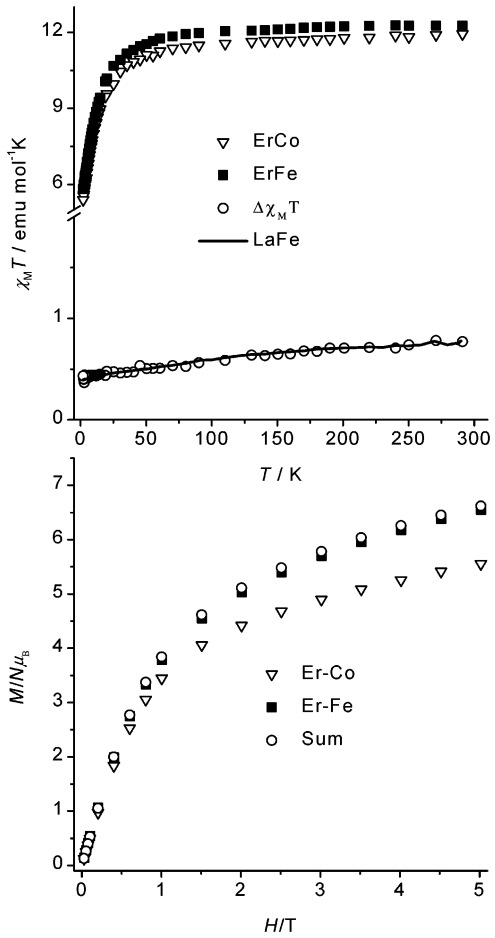

Figure 4. Top: thermal dependence at 0.1 T of $\chi_M^{ErFe}T$, $\chi_M^{ErCo}T$, $\chi_M^{LaFe}T$, and $\Delta\chi_M T = \chi_M^{ErFe}T - \chi_M^{ErCo}T$. Bottom: magnetization vs H of M^{ErFe}, M^{ErCo} at 2 K, and sum $= M^{ErCo} + M^{LaFe}$.

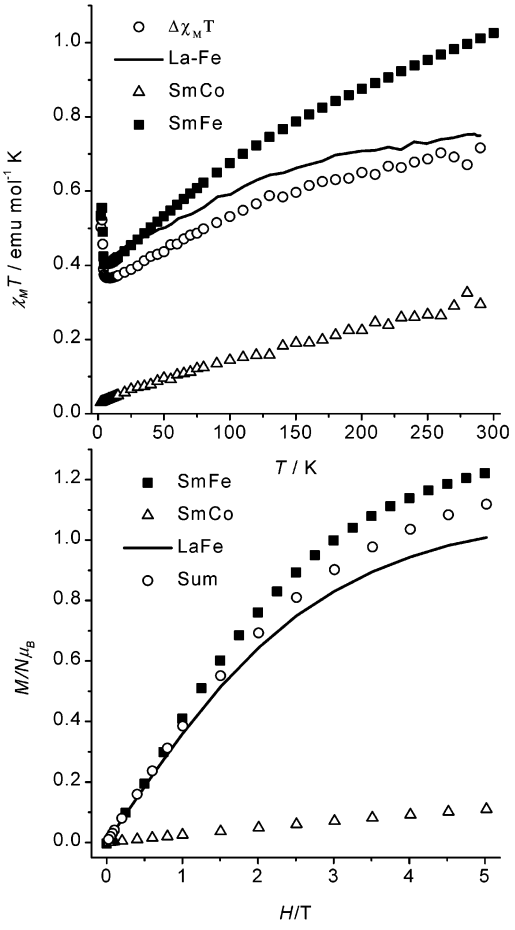

Figure 5. Top: thermal dependence at 0.1 T of $\chi_M^{SmFe}T$, $\chi_M^{SmCo}T$, $\chi_M^{LaFe}T$, and $\Delta\chi_M T = \chi_M^{SmFe}T - \chi_M^{SmCo}T$. Bottom: magnetization vs H of M^{SmFe}, M^{SmCo}, M^{LaFe} at 2 K, and sum $= M^{SmCo} + M^{LaFe}$.

earth series. As an example, the decrease in the cell parameter *c* is shown in Supporting Information, Figure S2.

NMR Studies. NMR studies were carried out on the new $Ln^{3+}-Co^{3+}$ family to complete their characterization. Only signals due to free *N*,*N*′-dimethylformamide were found when the proton NMR spectra of solutions of the $Ln^{3+}-Co^{3+}$ compounds were recorded in D_2O solutions. This result shows the compounds' great lability in aqueous solution. It should be noted that no signals due to the coordinated ligand were found, even when some drops of deuterated *N*,*N*′-dimethylformamide were added to the solution. Because of the lability of this complex in solution, the ^{13}C CP-MAS NMR spectra were carried out in the solid state. The spectrum of the diamagnetic $[La^{3+}-Co^{3+}]$ complex shows two signals corresponding to NMe_2 carbons at $\delta = 36.2$, 41.9, because of the different disposition of these groups in relation to the CO fragment. The crystal structure of the complexes $[Yb^{3+}-Co^{3+}]$ (**3**), $[Ce^{3+}-Co^{3+}]$ (**4**), and $[Sm^{3+}-Co^{3+}]$ (**5**) shows that one methyl group is in a *syn* position in relation to the CO group and the other methyl group is in an *anti* position. A signal at 169.2 ppm due to the HCO carbon is also observed. The ^{13}C NMR spectra of the paramagnetic complexes, in the solid state, show two signals corresponding to NMe_2 carbons at $\delta = 30.0$, 40.1; and 36.9, 44.3 for the $[Ce^{3+}-Co^{3+}]$ and $[Sm^{3+}-Co^{3+}]$ complexes, respectively. A broad signal at $\delta = 41.5$, 40.0, and 39.3 was observed for the $[Pr^{3+}-Co^{3+}]$, $[Nd^{3+}-Co^{3+}]$, and $[Eu^{3+}-$

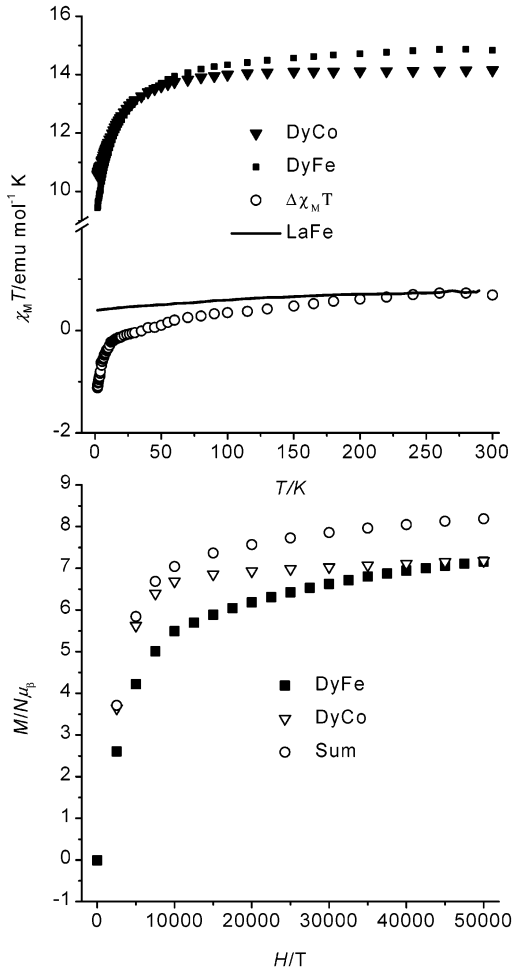

Figure 6. Top: thermal dependence at 0.1 T of $\chi_M{}^{DyFe}T$, $\chi_M{}^{DyCo}T$, $\chi_M{}^{LaFe}T$, and $\Delta\chi_M T = \chi_M{}^{DyFe}T - \chi_M{}^{DyCo}T$. Bottom: magnetization vs H of M^{DyFe}, M^{DyCo} at 2 K, and sum $= M^{DyCo} + M^{LaFe}$.

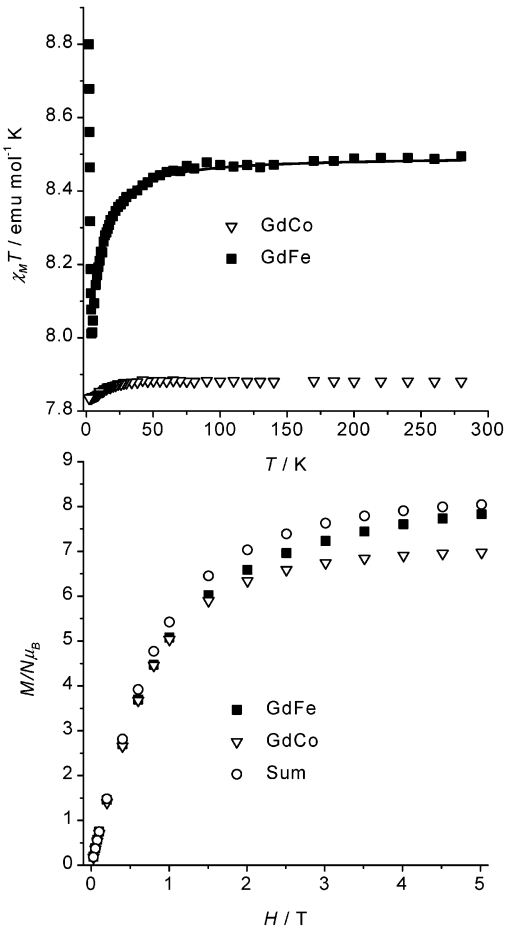

Figure 7. Top: thermal dependence at 0.1 T of $\chi_M{}^{GdFe}T$, $\chi_M{}^{GdCo}T$. The solid line represents the best fitting (see text for the fitted parameters). Bottom: magnetization vs H of M^{GdFe}, M^{GdCo} at 2 K, and sum $= M^{GdCo} + M^{LaFe}$.

Co^{3+}] compounds, respectively. A broad signal, due to the H−C═O carbon, is also observed at δ values between 190 and 130 ppm, in the NMR spectra of [Ce^{3+}−Co^{3+}], [Pr^{3+}−Co^{3+}], and [Nd^{3+}−Co^{3+}] compounds. No signals were observed for the complexes of the heavy elements of the lanthanide−cobalt family: Gd, Tb, Dy, Ho, Er, Tm. Only the spectrum of the [Yb^{3+}−Co^{3+}] complex presents three broad signals at 186.0, 115.5, and 30.2 ppm. The difference between the first and the second half of the lanthanide−cobalt family in their ^{13}C NMR spectra should be noted. Signals due to NMe_2 carbons can be observed in all the complexes of the first half of the family, but in contrast, the only complex of the heavy lanthanides of the series that shows signals in its NMR spectrum is the [Yb^{3+}−Co^{3+}] complex. The lanthanides have frequently been reported to behave as two distinct groups with a break between the lighter elements and the heavier elements. The origin of this break is not well-understood, but structural changes, variations in the hyperfine coupling constants, and changes in nonaxial pseudo-contact-shift contributions along the lanthanide series have been suggested as possible explanations.[36,37] As an example, the ^{13}C NMR spectra of [Yb^{3+}−Co^{3+}], [Pr^{3+}−Co^{3+}], and [Sm^{3+}−Co^{3+}] are shown in Supporting Information, Figure S3.

Magnetic Study. Informative magnetic measurements were performed for the 25 lanthanide−iron and lanthanide−cobalt complexes. In these complexes, the lanthanide (with the exception of Gd^{3+}) and iron ions possess a first-order angular momentum, which prevents the use of a spin-only Hamiltonian for isotropic exchange. This is the reason we investigated the possibility of a more empirical approach. The approach used in obtaining new insights on the nature of the Ln^{3+}−$Fe^{3+}{}_{LS}$ metal ion interaction consists of comparing the magnetic susceptibility data of isostructural Ln^{3+}−$Fe^{3+}{}_{LS}$ and Ln^{3+}−Co^{3+} compounds together with the magnetic properties of the [La^{3+}−Fe^{3+}] in order to take into account the anisotropy of the Fe^{3+} ion. The Co^{3+} ion and the La^{3+} ion are obviously diamagnetic, and the deviation of the magnetic susceptibility of these compounds with respect to the Curie law is due entirely to the thermal population of the Ln^{3+} Stark components and the anisotropy of $Fe^{3+}{}_{LS}$, respectively. Accordingly, an increase of the $\Delta\chi_M T = \chi_M{}^{LnFe}T - \chi_M{}^{LnCo}T$ when the temperature is lowered is indicative of a ferromagnetic Ln^{3+}−$Fe^{3+}{}_{LS}$ interaction, a decrease being indicative of an antiferromagnetic interaction. Furthermore, in several cases, we compare our results by applying the same method in magnetization measurements

(36) Peters, J. A. *J. Magn. Reson.* **1986**, *68*, 240.
(37) Bertini, I.; Luchinat, C. *Coord. Chem. Rev.* **1996**, *150*, 1.

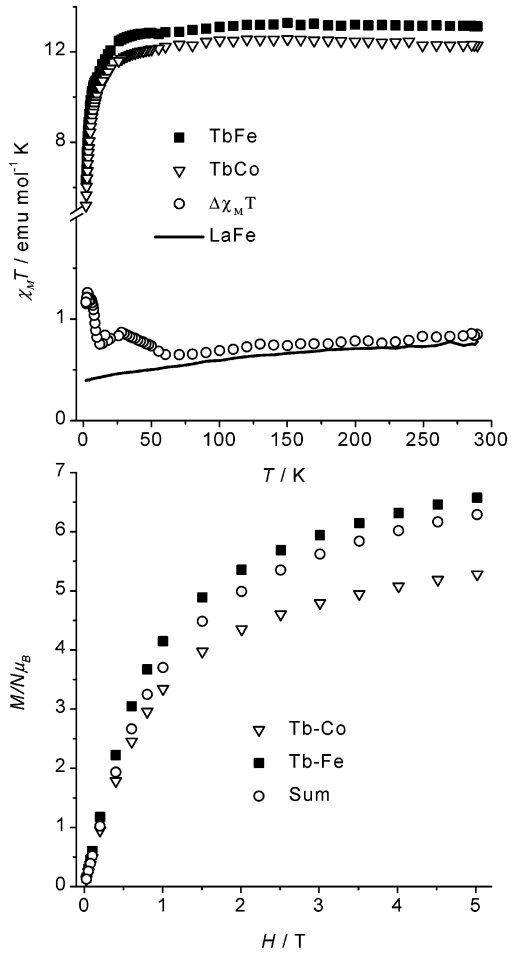

Figure 8. Top: thermal dependence at 0.1 T of $\chi_M{}^{TbFe}T$, $\chi_M{}^{TbCo}T$, $\chi_M{}^{LaFe}T$, and $\Delta\chi_M T = \chi_M{}^{TbFe}T - \chi_M{}^{TbCo}T$. Bottom: magnetization vs H of M^{TbFe}, M^{TbCo} at 2 K, and sum $= M^{TbCo} + M^{LaFe}$.

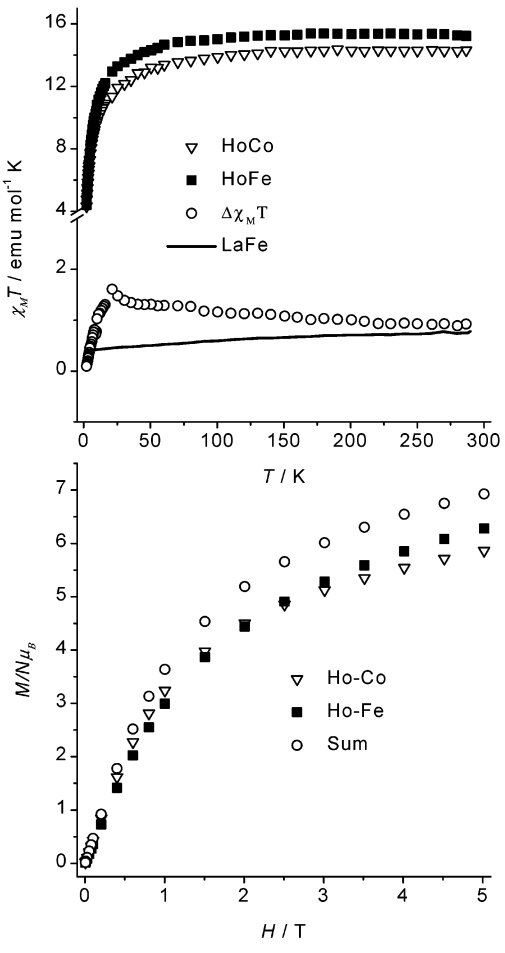

Figure 9. Top: thermal dependence at 0.1 T of $\chi_M{}^{HoFe}T$, $\chi_M{}^{HoCo}T$, $\chi_M{}^{LaFe}T$, and $\Delta\chi_M T = \chi_M{}^{HoFe}T - \chi_M{}^{HoCo}T$. Bottom: magnetization vs H of M^{HoFe}, M^{HoCo} at 2 K, and sum $= M^{HoCo} + M^{LaFe}$.

of the same compounds. More explicitly, the experimental magnetization of every $Ln^{3+}-Fe^{3+}{}_{LS}$ compound is compared with the sum of the $Ln^{3+}-Co^{3+}{}_{LS}$ and $[La^{3+}-Fe^{3+}{}_{LS}]$ magnetization curves, that is, the uncorrelated spin systems.

Three types of behavior are observed in the lanthanide−iron family: negligible, antiferromagnetic, and ferromagnetic interaction. This division takes into account only the intramolecular interactions. In some cases, at very low temperature, intermolecular interactions take place through hydrogen bonds.

(a) Negligible Interaction: $[Ln(DMF)_4(H_2O)_3(\mu\text{-}CN)Fe(CN)_5]\cdot nH_2O$ (Ln^{3+} = Pr, Eu, Er, Sm, Yb). For the case of $[Er^{3+}-Fe^{3+}]$ (Figure 4), $\Delta\chi_M T$ is superimposable with $\chi_M{}^{LaFe}T$, indicating that there is negligible interaction between the spin carriers. The experimental magnetization of $[Er^{3+}-Fe^{3+}]$ at 2 K (Figure 4) is also superimposable with the uncorrelated spin system. This negligible interaction seems to be for $[Eu^{3+}-Fe^{3+}]$ (Eu^{3+} has a nonmagnetic ground state, $^7F_0$), $[Pr^{3+}-Fe^{3+}]$ (in which case the ground term $^3H_4$ of Pr^{3+} gives rise to a singlet ground Stark level, as it is a non-Kramer ion), $[Yb^{3+}-Fe^{3+}]$ (Supporting Information, Figures S4−S6, respectively), and $[Sm^{3+}-Fe^{3+}]$. For the $[Sm^{3+}-Fe^{3+}]$ complex, from room temperature (rt) to 7 K the $\Delta\chi_M T$ and $\chi_M{}^{LaFe}T$ curves are quasiparallel (Figure 5). At low temperatures (from 7 to 2 K), important interdimer interactions take place because of the strong hydrogen bonding leading to an abrupt rise in $\Delta\chi_M T$. Furthermore, the experimental magnetization of $[Sm^{3+}-Fe^{3+}]$ at 2 K (Figure 5) is higher than that of the uncorrelated spin system. Possibly, the mentioned interaction due to hydrogen bonds is ferromagnetic.

(b) Antiferromagnetic Interaction: $[Ln(DMF)_4(H_2O)_3(\mu\text{-}CN)Fe(CN)_5]\cdot nH_2O$ (Ln^{3+} = Ce, Nd, Gd, Dy). For the case of $[Dy^{3+}-Fe^{3+}]$, the temperature dependence of $\chi_M{}^{DyFe}T$, $\chi_M{}^{DyCo}T$, and $\Delta\chi_M T$ is shown in Figure 6. To understand the importance of the anisotropy of $Fe^{3+}{}_{LS}$, the susceptibility data of $[La^{3+}-Fe^{3+}]$, $\chi_M{}^{LaFe}T$, is also shown in the same figure. From approximately 100 K, $\Delta\chi_M T$ decreases with regard to the $\chi_M{}^{LaFe}T$ curve. This profile of the $\Delta\chi_M T$ curve clearly shows that weak antiferromagnetic interactions take place. Furthermore, the experimental magnetization of $[Dy^{3+}-Fe^{3+}]$ at 2 K (Figure 6) is lower than that of the uncorrelated spin system, corroborating the antiferromagnetic coupling. For the $[Gd^{3+}-Fe^{3+}]$ complex, the temperature dependence of $\chi_M{}^{GdFe}T$ and $\chi_M{}^{GdCo}T$ is shown in Figure 7. The isotropic nature of Gd^{3+} helps to directly investigate the $\chi_M{}^{GdFe}T$ curve where it is clear that the interaction is antiferromagnetic. The value of $\chi_M{}^{GdFe}T$ at room temperature is 8.5 emu mol^{-1} K (close to the value expected for two uncorrelated spins $S = {}^7/_2$ and $S = {}^1/_2$; the room temperature value of $\chi_M{}^{LaFe}T$ is 0.7

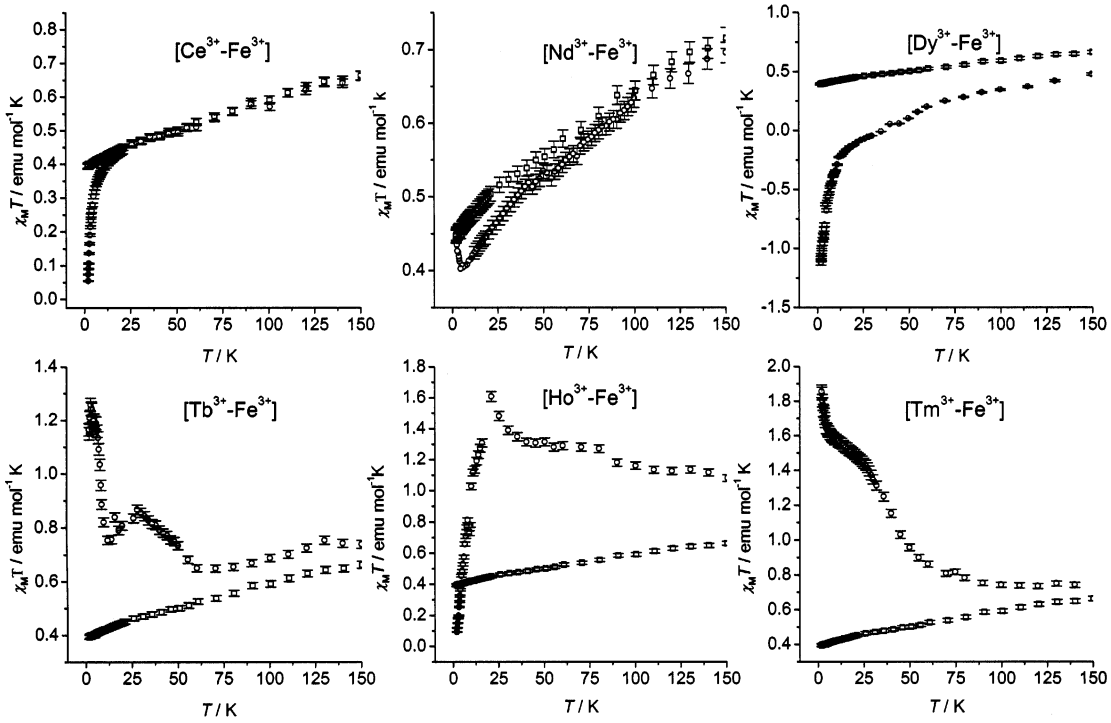

Figure 10. Top (antiferromagnetic coupling): thermal dependence (150−2 K) at 0.1 T, indicating via error bars the uncertainty in the plots of $\chi_M{}^{LaFe}T$ (□), $\Delta\chi_M T = \chi_M{}^{LnFe}T - \chi_M{}^{LnCo}T$ (Ln = Ce, Nd, Dy, ○). Bottom (ferromagnetic coupling): thermal dependence (150−2 K) at 0.1 T, indicating via error bars the uncertainty in the plots of $\chi_M{}^{LaFe}T$ (□), $\Delta\chi_M T = \chi_M{}^{LnFe}T - \chi_M{}^{LnCo}T$ (Ln = Tb, Ho, Tm, ○).

emu mol^{-1} K). But at the minimum, this value is 8.0 emu mol^{-1} K, later increasing to the value of 8.7 emu mol^{-1} K at 2 K. This feature may be due to ferromagnetic interdimer interactions, due to hydrogen bonds. The experimental magnetization of [Gd^{3+}−Fe^{3+}] (Figure 7) is lower than that of the uncorrelated spin system. Therefore, we propose that the antiferromagnetic intradimer interaction is in this case the dominant interaction at 2 K. To investigate the exchange interaction of the system, the following Hamiltonian formalism was used to fit the susceptibility data in the temperature range 10−300 K and thus avoid interdimer interactions:

$$H = JS_1S_2 + \sum_{i=1-2} H\beta g_i S_i \qquad (1)$$

The g values of the Fe^{3+} were taken from EPR measurements of the [La^{3+}−Fe^{3+}] complex (Supporting Information, Figure S7) and are $g_{xy} = 2.0$, $g_z = 2.47$ (at 2 K), while the g value of Gd^{3+} was kept fixed at $g = 2.0$. The fitting result is shown in the same figure as a solid line; the value of the exchange interaction is $J = 0.5$ cm^{-1}, showing that a small antiferromagnetic interaction exists between the ions. For the case of [Ce^{3+}−Fe^{3+}], the $\chi_M{}^{LaFe}T$ being almost superimposable to the $\Delta\chi_M T$ to 25 K, after which temperature $\Delta\chi_M T$ decreases to the value of 0.02 cm^3 mol^{-1} K. The profile of the $\Delta\chi_M T$ curve clearly shows that weak antiferromagnetic interaction takes place (Supporting Information, Figure S8). Finally, in the case of [Nd^{3+}−Fe^{3+}], a very small antiferromagnetic coupling is observed through susceptibility and magnetization measurements (Supporting Information, Figure S9).

(c) Ferromagnetic Interaction: [Ln(DMF)$_4$(H$_2$O)$_3$(μ-CN)Fe(CN)$_5$]·nH$_2$O (Ln^{3+} = Tb, Ho, Tm). The case of [Tb^{3+}−Fe^{3+}] is investigated in Figure 8. While $\Delta\chi_M T$ is almost superimposable to $\chi_M{}^{LaFe}T$ until 50 K, it rapidly increases below that temperature and leads to a ferromagnetic [Tb^{3+}−Fe^{3+}] interaction. Magnetization measurements (Figure 8) also prove the above argument because the experimental magnetization of [Tb^{3+}−Fe^{3+}] is higher than that of the uncorrelated spin system. The case of [Tm^{3+}−Fe^{3+}] is the same (Supporting Information, Figure S10). The magnetic behavior of [Ho^{3+}−Fe^{3+}] is different and is shown in Figure 9. $\Delta\chi_M T$ is higher that $\chi_M{}^{LaFe}T$ and increases inversely with the temperature until 25 K. This reflects a possible ferromagnetic character of the [Ho^{3+}−Fe^{3+}] interaction, where an abrupt decrease occurs, leading to a value near zero at 2 K (possibly due to interdimer antiferromagnetic interactions). These interdimer interactions are reflected in the magnetization data (Figure 9) where, at 2 K, the experimental [Ho^{3+}−Fe^{3+}] curve is lower than that of the uncorrelated spin system.

The uncertainty for all measurements could be important in this kind of small coupling. To avoid any misinterpretation, the $\chi_M T$ values in the low temperature zone (150−2 K) with their uncertainties in the plot, via error bars, are given in Figure 10, showing that the errors in the measurements do not affect the sign of the coupling.

Discussion

According to this study, the Ln^{3+}−Fe^{3+} interaction is antiferromagnetic for the cases of Ln^{3+} = Ce, Nd, Gd, and Dy but ferromagnetic for the cases of Ln^{3+} = Tb, Tm, and Ho. The cases of Ln = Pr, Eu, Er, Sm, and Yb have negligible interaction with the Fe^{3+} ion. Costes et al.[8] has introduced a new approach which gives information on the type of interaction (ferro- or antiferromagnetic). This empiri-

Table 3. Nature of the Magnetic Interaction between Ln^{3+} and Fe^{3+} and Comparison with Other Pairs

LnFe	Ce	Pr	Nd	Sm	Eu	Gd	Tb	Dy	Ho	Er	Tm	Yb
Ni_3Ln_2[a]	PAF	PAF	PAF	PAF	PAF	F	F	F	F	?	?	?
Cu_3Ln_2[b]	PAF	PAF	PAF	PAF	PAF	F	F	F	?	?	F	?
CuLn[c]	AF	NI	AF	AF	NI	F	F	F	F	F	AF	AF
FeLn[d]	AF	NI	AF	NI	NI	AF	F	AF	F	NI	F	NI

[a] Ref 38. PAF = proposed antiferromagnetic interaction; F = ferromagnetic interaction; AF = antiferromagnetic interaction; NI = negligible interaction; ? = unresolved interaction. [b] Ref 2. [c] Ref 8. [d] This work.

cal approach is based on a comparison of the magnetic properties of homologous $[LCu(Me_2CO)Ln(NO_3)_3]$ and $[LNi(Me_2CO)Ln(NO_3)_3]$ dinuclear complexes in which the nickel centers are diamagnetic. This comparison is needed in order to eliminate the crystal field contribution of Ln ions in the pairs, and the resulting behavior was attributed to intramolecular magnetic interactions. The $Cu^{2+}-Ln^{3+}$ interaction is antiferromagnetic for Ln = Ce, Nd, Sm, Tm, and Yb, and ferromagnetic for Ln = Gd, Tb, Dy, Ho, and Er. However, the $[Cu^{2+}-Pr^{3+}]$ and the $[Cu^{2+}-Eu^{3+}]$ pairs are devoid of any significant interaction. The same empirical approach but with different conclusions was used by Kahn et al.[2,38] in a series of compounds with the general formula $[Ln_2[M(obpa)]_3]\cdot S$. Here, S stands for solvent molecules, obpa for *ortho*-phenylenebis(oxamato), and M = Cu, Zn, Ni. These structures consist of infinite ladder-type motifs where the side pieces of the ladders are made of Ln[M(obpa)] units, and the rungs are made of [M(obpa)] units that bridge two Ln atoms belonging to either side piece. In the first half of the lanthanide series, all the complexes were found to be antiferromagnetically coupled to the Cu^{2+}. The Gd^{3+}, Tb^{3+}, Tm^{3+}, and Dy^{3+} complexes are ferromagnetically coupled, while an uncertainty remains regarding all the rest. Table 3 summarizes all these compounds and includes our new findings concerning the Ln−Fe dimers. The significant differences between the previous results and the present work are the cases of Gd^{3+} and Dy^{3+} which yield antiferromagnetic interaction in contrast to the previous compounds. It may be due to two main reasons: (a) the anisotropic character of the Fe^{3+} ion and (b) the CN^- bridging. Unfortunately, the hydrogen bonds in the net can give important intermolecular interactions which hide the $Ln^{3+}-Fe^{3+}$ intramolecular interactions at low temperature. Thus, further studies are necessary to synthesize and characterize new isolated dinuclear complexes to corroborate and contrast all these results.

Acknowledgment. This work was financially supported by Spanish Government (Grant BQU2000-0791).

Supporting Information Available: Additional table, figures and crystallographic data in CIF format. This material is available free of charge via the Internet at http://pubs.acs.org.

IC025669G

(38) Kahn, M. L.; Lecante, P.; Verelst, M.; Mathoniere, C.; Kahn, O. *Chem. Mater*. **2000**, *12*, 3073.